MRI Bias Field Correction Based on Tissue Labeling

Lianli Liu, Jiyang Chu*, Jie Li, Zhen Zeng
Electrical Engineering and Computer Science, University of Michigan.
Nuclear Engineering and Radiological Sciences, University of Michigan*.
Ann Arbor, MI 48109
{llliu,chujy,ljlijie,zengzhen}@umich.edu
EECS 556 Feb 28th 2014

I. Introduction

Intensity nonuniformities, also known as bias field in magnetic resonance (MR) imaging arises from various factors such as imperfections in the radiofrequency (RF) pulse profile; nonuniform flip angles caused by an inhomogeneous transmit field; nonuniform reception sensitivity; RF penetration effects dependent upon the electromagnetic parameters of the object ;wave behavior when the object size is equal to or more than one-half the wavelength of electromagnetic radiation and finally, gradient eddy currents related to the coupling between the object and gradient coils [1]. Such bias field manifests as a slowly varying signal intensity variation across tissue regions that should be uniform, as shown in Fig1. Human eyes are not sensitive to such intensity inhomogeneity that is why medical experts can perform analysis tasks correctly. However, many intensity based image analysis algorithms are very sensitive to such intensity variation, thus correction of bias field is of great importance for accurate image analysis results.

Various methods have been proposed to address this issue, including prospective methods [2][3][4], where bias field is corrected during imaging and retrospective ones, where bias field is estimated from images. Retrospective methods are more general in application as they do not rely on specific MR scanners and are able to remove patient induced inhomogeneity.

However, most existing retrospective methods only rely on image intensities or simple statistics referred from intensities [5][6][7] , other useful information, such as geometric shape, texture are ignored. In this project, we investigate the utility of more complicated features in bias field correction. Techniques developed in computer vision are introduced to discover more prior knowledge of image that may guide bias correction better. And our hypothesis are

- Segmentation and bias field estimation are two interacting factors, and improving one will enhance the other.
- Encountering more complicated features other than simple pixelwise intensity will improve segmentation.

And we will also investigate the regularization scheme since bias estimation is an ill posed problem that requires proper regularization.

II. Related Work

A. Segmentation Based Bias Field Correction

Among various retrospective methods, segmentation based methods have received much attention as they incorporate anatomy information, i.e. tissue type into correction process. For example, maximum-likelihood (ML) or maximum a posteriori probability (MAP) criterion are applied to estimate image intensity probability distributions by parametric modes, where bias field is modeled as a Gaussian mixture model as in [8][9]. Fuzzy c-means based segmentation is also insensitively studied as it assigns partial membership to voxels, which is consistent with partial volume effect in MR images. Standard fuzzy c-means objective function is modified in various ways to incorporate bias field effect [10][11][12]. Other methods based on non parametric models are also proposed as in [13][14], using maxshift or meanshift clustering.

All these methods rely on image intensity only for segmentation, while over the past few decades, image segmentation has been an active area in computer vision, where numerous methods have been proposed that rely on more complicated features extracted from image instead of simple pixel intensity.

B. Image Segmentation

Image segmentation is the process of partitioning a digital image into multiple segments. The goal of segmentation is to simplify and/or change the representation of an image into something that is more meaningful and easier to analyze. It has long been investigated in the field of image processing and computer vision. Depending on whether prior information is provided, image segmentation can be categorised into unsupervised segmentation and supervised segmentation. Unsupervised segmentation clusters pixels based on their similarities in specific aspects (features). Examples of the specific aspects being used in computer vision community are color of a pixel, or richer features such as texture and shapes. Felzenszwalb [15] et.al. proposed a graph-based algorithm to segment an image into regions. They start with a graph with each node corresponding to each pixel, and each pixel is connected to its neighbours by edges. Then they iteratively prune the edges if two connected components are dissimilar. The final graph with separated connected components correspond to separate regions in the segmentation result. Their work presented good

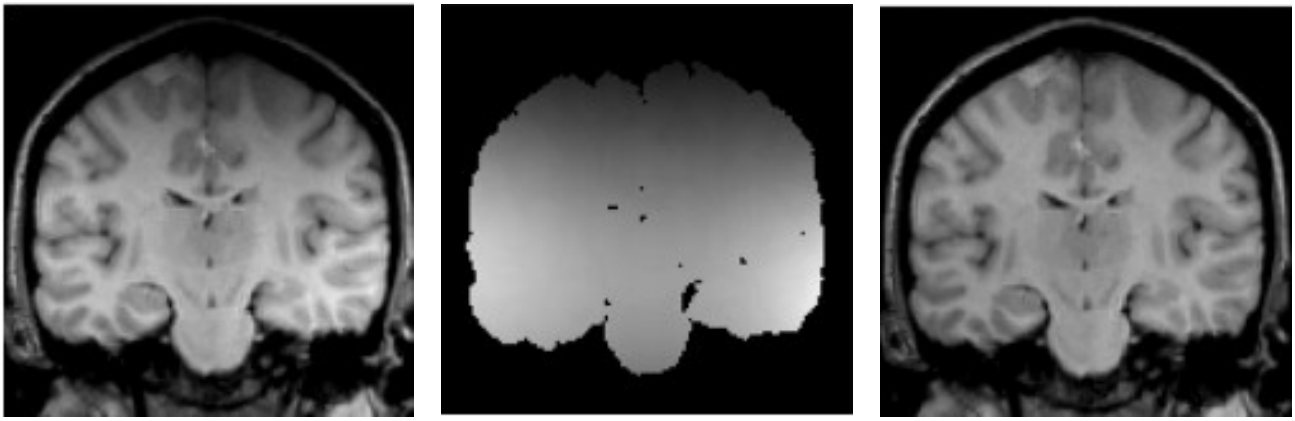

(a) Image corrupted by bias fiedl (b) Estimated bias field (c) Corrected image

Figure 1. Illustration of bias field

segmentation results that align with the visual boundaries, but an image can be oversegmented in a sense that each segment does not correspond to a semantic entity, such as an object.

If we want to get semantic level segmentation, such as object segmentation, then prior knowledge on the object could be utilized for better segmentation. Supervised segmentation grouped pixels into regions such that each region get assigned to a specific pre-trained semantic label. These methods typically start with oversegmentation results of an image, and then learn a prior on the appearance for each semantic label, so that they can estimate the posterior probability of assigning a specific label to one segment based on the appearance of the segment. Derek et.al. [16] learned the appearance model for some 3D geometric labels, such as "horizontal" and "vertical". Their work segment a given image into several geometric classes. The features that they used are simple and several 3D geometric features designed specifically for their task. In the case that hand crafted features are powerful enough, we can deploy deep learning [17] algorithm to automatically generate a hierarchy of useful features. Farabet et.al. [17] used deep learning for generating a set of features in the task of scene labeling. The drawback of this line of work is the requirement of a huge amount of training data, which is hard to get due to the human efforts needed on labeling.

To conclude, The general hypothesis behind segmentation based methods are

1) Accurate segmentation and correct bias field estimation are two interacting factors, improve one will lead better result in the other:

2) Bias field estimation is an ill posed problem that requires proper regularization: On the other hand, various segmentation algorithms developed in computer vision rely on the hypothesis that considering more complicated features other than simple voxel intensity will improve segmentation based bias field correction methods.

In this project we will investigate more deliberate segmentation methods for better bias field correction, as well as the corresponding regularization schemes.

III. Proposed Method

In this project we investigate more deliberate segmentation methods for better bias field correction, and we will adpat the regularization shemes in the bias field correction accordingly.

A. Rich Feature Tissue Segmentation

We aim to segment a given MRI image into regions that correspond to four tissue types, i.e., solid tissue, water, fat, and bone. Appearance based features can be extracted to model each class. Integrating different features into a segmentation process is not a trivial task. Different features ask for different spatial support. Some are small-scale features like color or texture. Some are large-scale features like SIFT or SURF. How to provide the supporting area largely affects the robustness and accuracy of an segmentation algorithm. Inspired by the work of Derek et al citehoiem2005geometric scene labeling, we proposed to use multi-level segmentation to address this problem.

As shown in Fig 2, our proposed algorithm falls into 4 parts: 1) Superpixel generation; 2) Multiple hypothesis generation; 3) Tissue Labeling; 4) training.

1) Superpixel Generation: We directly apply the segmentation methods by Felzenszwalb [15] to get a set of over segmented superpixels. The goal of the tissue segmentation is to label each superpixel as one of the pre-defined tissue classes.

2) Multiple Hypothesis Generation: By changing the thresholds in the segmentation methods [15], we can have different oversegmentation results. It is intractable to evaluate every possible oversegmentation result and find the one that best segments the image into the pre-learned classes. Thus we will first group the superpixels of the oversegmentation into bigger regions based on some their features similarities. And the number of the final regions after the grouping can vary, thus we use different numbers of regions for different groupings of the regions, each referred as one of our hypothesis.

3) Tissue Labeling: For each hypotheses, we assume that each region belong to the same tissue class, meaning all the superpixels within that region should be assigned to the same tissue label. Because of multiple hypothesis, each superpixel

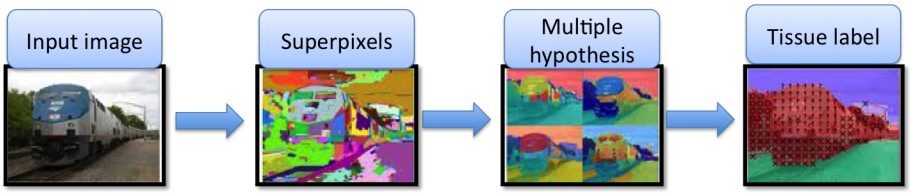

Figure 2. Tissue label pipeline [16]

will be a member of several different regions from different hypothesis. The superpixel label confidence 1 is measured by a weighted sum of the label likelihoods of the regions that contain it, and the weights depend on the homogeneity likelihood of the regions:

$$C(y_i = v|x) = \sum_{j}^{n_h} P(y_i = v|x, h_j i) P(h_j i|x) \qquad (1)$$

where y_i is the superpixel label, and v is one of the possible labels, and x is the image, n_h is the total number of hypothesis, and $h_j i$ is the regions that contains the $i^t h$ superpixel for the $j_t h$ hypothesis, and y_j is the tissue label for the region $h_j i$. The label likelihood function of the regions, and the homogeneity likelihood function of the regions are learned in our training stage, as explained below.

4) Training: In the training stage, for each training image, we generate multiple hypothesis. And for each hypothesis, we label the region as one of the pre-defined tissue class if the region corresponds well to one tissue class, or label the region as "mixed" if the region contains multiple tissue classes. Features are extracted within each region, and the features being used are as shown in Fig 3. Details about features extractions are explained later. The label likelihood function of a region given the image data within that region is learned in a one versus rest fashion. And the homogeneity likelihood function of a region is learned by classifying homogeneously labeled (i.e. label as just one of the tissue classes) vs "mixed" labeled. Both likelihood functions can be estimated using logistic regression version of Adaboost [18], or using other classifiers such as SVM [19].

Features As shown in Fig 3, we have several types of features that we can extract within each region. We chose this set of features since they can help recognize the tissue type as explained below.

Intensity: Different MRI image types (T1 weighted, T2 weighted, etc) have different tissue contrast, and one single MRI volume may not be sufficient to separate all tissue types. For example, it has been reported that and T2-weighted images was more sensitive to bone density variation compared to other MRI image types; calculated fat image using Dixon method has strong contrast of fat with other tissue yet is not capable of separating other tissue types [20]. Most existing bias field uses single phase image (mainly T1 only) [21], thus it may be meaningful to study bias field correction using multi phase images, utilizing characteristics of different MRI volume types. Here we represent the intensity using two intensity channels: T1, and T2, and calculate their mean (I1) and histograms (I2).

Feature Description
Intensity I1: <T1,T2> : mean I2: <T1,T2> : histogram
Texture X1: LM filters: mean absolute response (15 filters) X2: LM filters: histogram of maximum responses (15 bins)
Location L1: normalized x and y, mean L2: norm. x and y, 10th and 90th pctl
Shape S1: number of superpixels in region S2: normalized area in image

Figure 3. Features to extract

Texture: Texture gives us a cue for the tissue type. We apply a subset of the filter bank by Leung and Malik [22]. The textures are represented by the absolute filter response of each filter (X1) and the histogram of maximum responses over pixels within a segment (X2).

Location: Since MRI images using the same coil are mostly aligned togher, the location is a very strong cue of what the tissue type is. The location are represented by the normalized pixel locations of the tissue type: the mean of the locations (L1), and also the 10th and 90th percentile of the pixel position of a region in the image (L2).

Shape: The shape and extension of the region is another cue that we can utilize. We represent the extension of the region by the number of superpixels (S1), and the shape is roughly represented by the normalized area in the image (S2). Depending on the results, we might incorporate more discriminative features for shape later.

B. Integrate Segmentation into Bias Field Correction

Given the segmentation results in part A, bias field can be estimated based on the assumption that same tissue type have uniform intensity. At this stage, we are not confident that the segmentation algorithm described above is sensitive to intensity change or not. Therefore, we propose two strategy to incorporate segmentation into bias field correction, corresponding to the intensity-insensitive case and intensity-sensitive case.

Intensity Insensitive Case When segmentation is invariant to intensity change, bias field will have little impact on segmentation results. Thus we may rely on the segmentation results to generate a bias free image. Given the label of each

voxel u_{ik} and the prototype of each voxel c_i (which can be easily obtained from training images or expert knowledge), the voxel intensity z_k bias free image will be

$$z_k = \sum_{i=1}^{c} u_{ik} c_i \tag{2}$$

With this bias free image, we can easily estimate bias field as

$$\mathbf{b} = \mathbf{X}/\mathbf{Z} \tag{3}$$

Where X is original image and Z is bias free image constructed by Eq(3). However, the bias field estimation is an inverse problem and ill-posed. Therefore we apply the following regularized version, as proposed in [23]:

$$\hat{\mathbf{b}} = \arg\ \min \frac{1}{2}\|\mathbf{Z} - \mathbf{X}\mathbf{b}\|^2 + \frac{\lambda}{2}\|\mathbf{R}\mathbf{b}\|_2^2 \tag{4}$$

Where $\mathbf{R}$ is the finite differencing matrix to ensure the smoothness of estimated bias field. Following the algorithm proposed in [23], this problem can be solved efficiently using variable splitting and Augmented Lagrangian(AL) methods.

Intensity Sensitive Case Under this scenario, we cannot fully trust our segmentation results. Segmentation and bias correction have to be performed jointly for an optimal solution. To do this, we apply the fuzzy c-means version and define the following objective function

$$\begin{aligned} J(b) &= \sum_{i=1}^{c}\sum_{k=1}^{n} u_{ik}^m \|x_k/b_k - v_i\|^2 \\ \text{s.t. } &\sum_{i=1}^{c} u_{ik} = 1 \end{aligned} \tag{5}$$

After segmentation, a bias field is estimated using Eq (5) and the bias corrected image fed back into the segmentation algorithm to update u_{ik}. To guarantee the smoothness of bias field, a regularization scheme similar with Eq(4) is incorporated but implemented implicitly as B spline smoothing.

IV. Experiment Design

Our experiment consists of four parts: the selection of datasets, the method of segmentation, the application of our algorithm, and the evaluation of bias correction.

A. Datasets

We have two kinds of images that can be used in the experiment. The first one is the MR image with true bias field. We can obtain the images from several sources. It is obvious that the bias field correction for this kind of image is practical. However, there is a lack of good evaluation methods for the quality of the result. To overcome this disadvantage, the second choice of images is to use a MR image without bias field, and add the bias field artificially as Allison did in [23].

Thus we can compare the original image and our optimized result numerously (Standard Deviation or PSNR). In our experiment, we will use both image datasets to not only prove our algorithm working in practical environment but also get a precise analysis.

B. Method of segmentation

Inspired by the work of Hoiem, Efros and Hebert [16] we can design our method of segmentation in several steps as following (details will be developed in future):

1) Superpixels generation:
2) Multiple hypothesis generation:
3) Feature extraction:
4) Tissue label training:
5) Tissue label testing:

C. Application of algorithm

First of all, we have obtained the initial segmented image from previous step. Then the segmentation based bias field correction algorithm can be conducted on the image. As the initial segmented image contains more information than this step, we need to add a segment constraint condition to the optimize equation. So the additional information from previous step can be kept while iterating. When the variables convergent, we can return to the previous step to do segmentation again, then conduct a new optimization. The loop is repeated until convergence of the segmentation or some other end conditions.

D. Evaluation of bias correction

For the image with true bias field, we can evaluate the result in two ways. The first one is directly comparing the original image and the corrected image by eyes. The second one is intensity coded segmentation result which is described by Vovk [21]. Our method is segmentation based, so intensity coded segmentation result is applicable.

For the image with artificial bias field, the quantitative evaluation is quite simple. After normalizing the bias corrected image, we can calculate the standard deviation or PSNR as the judgment of correction quality.

Finally we will discuss the advantages and disadvantages of our method, then draw some conclusions.

References

[1] J. Wang, M. Qiu, Q. X. Yang, M. B. Smith, and R. T. Constable, "Measurement and correction of transmitter and receiver induced nonuniformities in vivo," *Magnetic resonance in medicine*, vol. 53, no. 2, pp. 408–417, 2005.

[2] H. Watanabe, N. Takaya, and F. Mitsumori, "Non-uniformity correction of human brain imaging at high field by rf field mapping b+ of b- and," *Journal of Magnetic Resonance*, vol. 212, no. 2, pp. 426–430, 2011. http://www.sciencedirect.com/science/article/pii/S1090780711002588.

[3] H. Mihara, N. Iriguchi, and S. Ueno, "A method of rf inhomogeneity correction in mr imaging," *Magnetic Resonance Materials in Physics, Biology and Medicine*, vol. 7, no. 2, pp. 115–120, 1998. http://www.sciencedirect.com/science/article/pii/S1352866198000672.

[4] K. P. Pruessmann, M. Weiger, M. B. Scheidegger, P. Boesiger, *et al.*, "Sense: sensitivity encoding for fast mri," *Magnetic resonance in medicine*, vol. 42, no. 5, pp. 952–962, 1999. http://macduff.usc.edu/ee591/library/Pruessmann-SENSE.pdf.

[5] M. Styner, C. Brechbuhler, G. Szckely, and G. Gerig, "Parametric estimate of intensity inhomogeneities applied to mri," *Medical Imaging, IEEE Transactions on*, vol. 19, no. 3, pp. 153–165, 2000. http://ieeexplore.ieee.org/xpls/abs_all.jsp?arnumber=845174.

[6] J. G. Sled, A. P. Zijdenbos, and A. C. Evans, "A nonparametric method for automatic correction of intensity nonuniformity in mri data," *Medical Imaging, IEEE Transactions on*, vol. 17, no. 1, pp. 87–97, 1998. http://ieeexplore.ieee.org/xpls/abs_all.jsp?arnumber=668698.

[7] N. J. Tustison, B. B. Avants, P. A. Cook, Y. Zheng, A. Egan, P. A. Yushkevich, and J. C. Gee, "N4itk: improved n3 bias correction," *Medical Imaging, IEEE Transactions on*, vol. 29, no. 6, pp. 1310–1320, 2010. http://www.ncbi.nlm.nih.gov/pubmed/20378467.

[8] W. M. Wells III, W. E. L. Grimson, R. Kikinis, and F. A. Jolesz, "Adaptive segmentation of mri data," *Medical Imaging, IEEE Transactions on*, vol. 15, no. 4, pp. 429–442, 1996.

[9] A. H. Andersen, Z. Zhang, M. J. Avison, and D. M. Gash, "Automated segmentation of multispectral brain mr images," *Journal of neuroscience methods*, vol. 122, no. 1, pp. 13–23, 2002. http://ieeexplore.ieee.org/xpls/abs_all.jsp?arnumber=511747.

[10] M. N. Ahmed, S. M. Yamany, A. A. Farag, and T. Moriarty, "Bias field estimation and adaptive segmentation of mri data using a modified fuzzy c-means algorithm," in *Computer Vision and Pattern Recognition, 1999. IEEE Computer Society Conference on.*, vol. 1, IEEE, 1999. http://ieeexplore.ieee.org/xpls/abs_all.jsp?arnumber=786947.

[11] M. N. Ahmed, S. M. Yamany, N. Mohamed, A. A. Farag, and T. Moriarty, "A modified fuzzy c-means algorithm for bias field estimation and segmentation of mri data," *Medical Imaging, IEEE Transactions on*, vol. 21, no. 3, pp. 193–199, 2002. http://ieeexplore.ieee.org/xpls/abs_all.jsp?arnumber=996338.

[12] D. L. Pham and J. L. Prince, "An adaptive fuzzy c-means algorithm for image segmentation in the presence of intensity inhomogeneities," *Pattern Recognition Letters*, vol. 20, no. 1, pp. 57–68, 1999. http://www.sciencedirect.com/science/article/pii/S0167865598001214.

[13] B. Likar, J. Derganc, and F. Pernus, "Segmentation-based retrospective correction of intensity nonuniformity in multispectral mr images," in *Medical Imaging 2002*, pp. 1531–1540, International Society for Optics and Photonics, 2002. http://www.sciencedirect.com/science/article/pii/S0167865598001214.

[14] J. Derganc, B. Likar, and F. Pernus, "Nonparametric segmentation of multispectral mr images incorporating spatial and intensity information," in *Medical Imaging 2002*, pp. 391–400, International Society for Optics and Photonics, 2002. http://proceedings.spiedigitallibrary.org/proceeding.aspx?articleid=879732.

[15] P. F. Felzenszwalb and D. P. Huttenlocher, "Efficient graph-based image segmentation," *International Journal of Computer Vision*, vol. 59, no. 2, pp. 167–181, 2004. http://www.cs.cornell.edu/~dph/papers/seg-ijcv.pdf.

[16] D. Hoiem, A. A. Efros, and M. Hebert, "Geometric context from a single image," in *Computer Vision, 2005. ICCV 2005. Tenth IEEE International Conference on*, vol. 1, pp. 654–661, IEEE, 2005. http://ieeexplore.ieee.org/xpls/abs_all.jsp?arnumber=1541316&tag=1.

[17] C. Farabet, C. Couprie, L. Najman, and Y. LeCun, "Learning hierarchical features for scene labeling," *Pattern Analysis and Machine Intelligence, IEEE Transactions on*, vol. 35, no. 8, pp. 1915–1929, 2013. http://ieeexplore.ieee.org/xpl/articleDetails.jsp?arnumber=6338939.

[18] M. Collins, R. E. Schapire, and Y. Singer, "Logistic regression, adaboost and bregman distances," *Machine Learning*, vol. 48, no. 1-3, pp. 253–285, 2002. http://link.springer.com/article/10.1023/A:1013912006537.

[19] C. Cortes and V. Vapnik, "Support-vector networks," *Machine learning*, vol. 20, no. 3, pp. 273–297, 1995. http://link.springer.com/article/10.1007/BF00994018.

[20] S.-H. Hsu, Y. Cao, K. Huang, M. Feng, and J. M. Balter, "Investigation of a method for generating synthetic ct models from mri scans of the head and neck for radiation therapy," *Physics in medicine and biology*, vol. 58, no. 23, p. 8419, 2013. http://www.ncbi.nlm.nih.gov/pubmed/24217183.

[21] U. Vovk, F. Pernus, and B. Likar, "A review of methods for correction of intensity inhomogeneity in mri," *Medical Imaging, IEEE Transactions on*, vol. 26, no. 3, pp. 405–421, 2007. http://ieeexplore.ieee.org/xpls/abs_all.jsp?arnumber=4114560.

[22] T. Leung and J. Malik, "Representing and recognizing the visual appearance of materials using three-dimensional textons," *International Journal of Computer Vision*, vol. 43, no. 1, pp. 29–44, 2001. http://link.springer.com/article/10.1023/A:1011126920638.

[23] M. J. Allison, S. Ramani, and J. A. Fessler, "Accelerated regularized estimation of mr coil sensitivities using augmented lagrangian methods," *Medical Imaging, IEEE Transactions on*, vol. 32, no. 3, pp. 556–564, 2013. http://ieeexplore.ieee.org/xpls/abs_all.jsp?arnumber=6361300.